Modeling Non-Stationary Asymmetric Lens Blur By Normal Sinh-Arcsinh Model

Jang Jinhyeok

Department of Electrical Engineering

Graduate school of UNIST

2016

Modeling Non-Stationary Asymmetric Lens Blur By Normal Sinh-Arcsinh Model

Jang Jinhyeok

Department of Electrical Engineering

Graduate school of UNIST

Modeling Non-Stationary Asymmetric Lens Blur By Normal Sinh-Arcsinh Model

A research proposal
submitted to the Department of Electrical Engineering
in partial fulfillment of the
requirements for the degree of
Master of Science.

Jang Jinhyeok

12. 10. 2015

Approved by

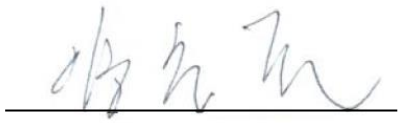

Advisor

Seungjoon Yang

Modeling Non-Stationary Asymmetric Lens Blur By Normal Sinh-Arcsinh Model

Jang Jinhyeok

This certifies that the research proposal of Jang Jinhyeok is approved.

12. 10. 2015

signature

Advisor: Seungjoon Yang

signature

Committee Member #1 : Jae-Young Sim

signature

Committee Member #2 : Se Young Chun

Abstract

Images acquired by a camera show lens blur due to imperfection in the optical system. Lens blur is non-stationary in a sense the amount of blur depends on pixel locations in a sensor. Lens blur is also asymmetric in a sense the amount of blur is different in the radial and tangential directions, and also in the inward and outward radial directions. This paper presents parametric blur kernel models based on the normal sinh-arcsinh distribution function. The proposed models can provide flexible shapes of blur kernels with different symmetry and skewness to model complicated lens blur accurately. Blur of single focal length lenses is estimated and the accuracy of the models is compared with existing parametric blur models. Advantage of the proposed models is demonstrated through deblurring experiments.

Contents

I. Introduction 1

II. Related Work 3

2.A Non parametric kernel estimation 3

2.B Skew model 5

2.C Optical aberrations 6

III. Contents 9

3.A Asymmetric Blur Model 9

3.B Asymmetric Blur Estimation 13

IV. Experiments and Discussion 15

4.A Asymmetric Blur Model 15

4.B Deblur with Asymmetric Blur Model 19

V. Conclusion 25

List of figures

Fig. 1. Results of each non-parametric blur estimation method

Fig. 2. Examples of the NSAS distribution function,

Fig. 3. Examples of kernel shapes of the NSAS and NEAS models at different parameters.

Fig. 4. Example of the test image for blur estimation

Fig. 5. 16 × 25 block-wise non-parametric estimation of blur kernels of a 35mm f/1.8 lens at aperture f/2.0.

Fig. 6. Blur kernels of a 35mm lens at aperture f/2.0 at locations of (a) cyan square and (b) yellow square in Fig. 4.

Fig. 7. Blur kernels provided by [8].

Fig. 8. Test images used in the SSIM experiment,

Fig. 9. CDF of SSIM error ratios at all the aperture values

Fig. 10. CDF of SSIM error ratios at aperture values wider than f/4

Fig. 11. Example of deblurred images in the SSIM experiment

Fig. 12. Example of deblurred images in the SSIM experiment

Fig. 13. Example of deblurred image with 35mm f/1.8 lens at aperture f/1.8

Fig. 14. Example of deblurred image with 50mm f/1.8 lens at aperture f/1.8

List of tables

Table I :
Parameters of the NSAS and NEAS models used for kernels in fig. 3

Table II :
Mse between the parametric kernels and non-parametric kernels estimated using a test pattern

Table III :
Mse between the parametric kernels and non-parametric kernels estimated using a random noise Pattern

Table IV :
Mse between the parametric kernels and measured non-parametric blur kernels from [8]

Modeling Non-Stationary Asymmetric Lens Blur By Normal Sinh-Arcsinh Model

Modeling Non-Stationary Asymmetric Lens Blur By Normal Sinh-Arcsinh Model

I. Introduction

Lens blur is a result of the imperfect optical system. Simply, a shown dot through a lens has larger and asymmetric shape whose boundaries are faded out. In the filter's view, blur is a kind of low-pass filter. Each location's data is affected on neighbor's data. This effect is a kind of weighted averaging, and ignores the detail components. In frequency domain, a low-pass filter, which is the blur in spatial domain, cuts out the high frequency components, which is detail components in spatial domain. This loss of detail information makes degradation.

Blur estimation is a research topic to measure PSF(Point Spread Function) of blur in any ways. This PSF is mathematical expression of the blur, used as filter in convolution. There are two subjects in blur estimation, one is blind estimation which estimates blur psf using captured images. The other one is estimating blur using any pattern and applying estimated psf into the real images. Many blind estimation methods use edge-detection or point-detection to use them as a main clue to estimate blur. Measurement from pattern images estimates PSF by comparing captured pattern image and groundtruth pattern image. By detecting blur PSF, it is possible to deblur blurred images. Deblurring is deconvolution to reconstruct high frequency components. It is possible to reconstruct perfect image if we know accurate PSF and there is no noise. This is a simple equation of deconvolution.

Most of the debluring methods are using this equation as data term and addtitional smoothness term. Therefore, it is important to estimate blur for the better deconvolution.

However, the estimated blur is too big to store and to use in real world. Also, there are some noise in PSF because of the noise of captured images. Every captured image by a camera has some noise because of imperfection of electrical system. A camera sensor should recognize only light, but recognize many other elements, like heat, as light. Moreover, the camera amplificates their sensor data in many cases and this makes more noise. Necessarily, estimating blur using these noised images makes noised results. Therefore, we modeled into parametric blur from estimated blur (non-parametric blur) by minimizing MSE(Mean Squared Error). This modeling makes two advantages, one is small memories to save blur data. The other one is much smoother blur PSFs.

Many researchers use Gaussian distribution for parametric modeling. However, a real blur is not symmetric. This means that Gaussian distribution is not sufficient to model real psfs. Many real psfs have skewnesses and tails, but Gaussian distribution cannot express them. For more accurate modeling, new distribution which can express skewness is necessary. For Simpkins et al. example,

Simpkins applied skew normal distribution into this modeling[9]. Not only this blur cases, also other many real cases, mainly in statistics, show skewed distribution. Therefore, there are many researches about skew distribution. Azzalini suggested a skewed distribution which is composed of multiplication between psf(possibility density function) and cdf(cumulative density function). The former one is for making main shape of distribution and the later one is for making skewness. Furthermore, there are skew T distribution, NSAS distribution, and another types of skew normal distributions.

In the optics, the blur is said as 'aberration.' Then there are many types of aberration, spherical aberration, astigmatism aberration, coma aberration, defocused aberration, field curvature aberration, distort aberration, and piston aberration[1]. Spherical aberration is due to differences in angles of incident light rays. Blur introduced by spherical aberration varies with the aperture size. Smaller aperture reduces marginal rays that travel through the edges of a lens, reducing the spherical aberration. Astigmatism is due to difference in focal points of meridional and sagittal rays. Blur introduced by astigmatism is asymmetric in a sense blur is more severe in one direction than the other. Coma is due to differences in magnification at different locations in a sensor. Blur by coma is more severe in the outward radial direction than the inward radial direction. Images captured with an optical system without astigmatism or coma may still show blur at the boundaries of a sensor frame because of the differences in focused points at different locations due to the field curvature. The blur coming from the field curvature is more severe at the boundaries of a sensor frame than at the center. Modern optical systems correct distortions through the arrangement of optical elements and through the use of sophisticated optical elements such as aspherical and extra low dispersion lenses [1], [2]. It is reported that images captured even with a sophisticated lens system under ideal conditions without camera shake or motion still show degradation [3], [4], [5], [6], [7], [8], [9], [10], [11]. The blur in images is non-stationary in a sense the amount of blur depends on the pixel locations in a sensor. The blur is asymmetric in a sense the amount of blur is different in the radial and tangential directions. Moreover, the blur is asymmetric in a sense that the amount of blur is different in the inward and outward radial directions. The point spread functions (psf's) or the blur kernels that represent lens blur show complicated shapes with elliptic contours with skewness.

In statistics, the skew-normal distribution and normal sinh-arcsinh (NSAS) distribution are used to model Gaussian-like distributions with skewness [12], [13], [14], [15]. Skew-normal distribution is obtained by multiplying the Gaussian density and the cumulative distribution together [12]. The skew-normal distribution retains the general shape of the Gaussian function with the skewness toward one direction. The NSAS distribution has two specific parameters that control the skewness and the kurtosis of the distribution [13], [14], [15]. The two dimensional NSAS distribution has more flexible shapes than the skew-normal distribution. In this paper, we use the two dimensional NSAS distribution to model the blur with the asymmetry and the skewness. The parameters inside the sinh function of

the NSAS distribution are separated into two separate groups of parameters in order to generalize the model further. The generalized model, named as the normal exponential-arcsinh (NEAS) model, can provide even more flexible shapes of blur kernel than the NSAS model. The NEAS model includes the NSAS model, and the NSAS model includes the Gaussian model. The proposed models are generalization of Gaussian model with simple choices of parameters.

Blur of a set of single focal length lenses at various pixel locations in a sensor at different aperture values is estimated and fitted by the proposed parametric blur models. The accuracy of the proposed models are evaluated and compared to other parametric lens blur models [3], [9] and other bivariate distributions that address skewness [12], [16]. The advantage of using the proposed models is demonstrated with deblurring experiments.

This paper is organized as follow. Section II reviews researches on estimation of non-stationary asymmetric lens blur. Section III-A introduces the parametric blur models based on the NSAS distribution function. Section III-B presents a method to estimate non-parametric and parametric asymmetric blur kernels. In section IV-A, the accuracy of the proposed models are evaluated. Section V concludes the paper.

II. Related Works

Lens blur can be measured using a point light source. In [5], a point source of a gas lamp is used to measure the psf's of a lens at specific locations in a sensor. In [8], a test pattern consists of point sources at rectangular grids displayed on a monitor is used to measure the psf's. Lens blur can be estimated from a photograph of a test pattern. In [6], [7], test patterns of particular shapes or random noise are photographed, and blur kernels are estimated by comparing the photographed image to mathematical definition of the test pattern.

A. non-parametric kernel estimation from pattern

1. Optimization estimation

This method is based on this equation.

$$Ax = b \tag{1}$$

In [3], researchers uses a Toeplitz matrix, a matrix whose diagonal components are constant, as A in that equation. Then, they set captured image as b, and find x using optimization. This x is a vectorized non-parametric blur kernel. In our approach, we used pseudo-inverse, and pseudo-inverse is faster minimizing MSE method. Therefore, both shows same kernels.

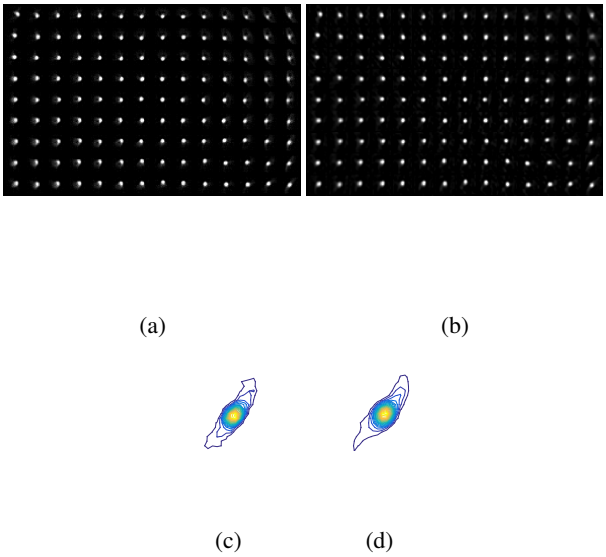

Fig. 1. Results of each non-parametric blur estimation method, (a),(b) : whole kernels, and (c),(d) : a kernel at left-bottom corner of Optimization and division in frequency domain

2. Division in frequency domain

As previously mentioned, convolution of blur kernel and original image makes blurred image. It can be expressed as

$$I * x = b \tag{2}$$

I is the original image, x is the kernel, and b is the blurred image. This can be expressed as

$$\frac{F(blurryimage)}{F(originalimage)} = F(blurkernel) \tag{3}$$

in frequency domain. Therefore, the x can be calculated as

$$F^{-1}(F(blurkernel)) = blurkernel \tag{4}$$

Only a problem is a case that there are 0s in frequency components of I. For preventing this, researchers uses noise patterns in [7].

The blur can be blindly estimated from a given photograph without specific knowledge of a lens or a camera [17]. However, the blur in a given image can be affected by many factors such as focusing distances to different objects or the movements of objects. It may be difficult to isolate the lens blur from the blur due to other factors. In these approaches, blur kernels are non-parametric. The shapes of blur kernels themselves are estimated and stored for future usage. Fig. 1 shows the similarity of two methods, In statistically, mean of the correlation of two methods' results is 0.9427, mean of the MSE is 0.0042, and mean of the Bhattacharyya distance is 0.0098. Those mean that two methods' results are much similar.

B. Skew model

1. Outside-Skewness models

Basically, Azzalini and Valle's Skew-Normal-Distribution model, there are such methods. Basic form of these models is like this, $f(x) = 2 \times pdf(x) \times cdf(x)$ Each models' names come from the kind of pdf and cdf. If the pdf and cdf were Gaussian's ones, f(x) would be a skew normal distribution. From pdf, these models make approximate shape and location. Then, they make skewness by the cdf. The examples of this method are skew-normal-distribution[12],[27], Skew-T-distribution[16], Simpkins' skew-normal-distribution model[9]. However, skew normal distributions cannot include normal distribution perfectly because of cdf-multiplication.

1-1. Bivariate skew normal distribution

$$f_2(x,y;\mu,\Sigma,D) = \frac{\exp\left(-\frac{1}{1-\rho^2}[\frac{(x-\mu_1)^2}{\sigma_1^2} - 2\frac{\rho(x-\mu_1)(y-\mu_2)}{\sigma_1\sigma_2} + \frac{(y-\mu_2)^2}{\sigma_2^2}]\right)}{2\pi\sigma_1\sigma_2\sqrt{1-\rho^2}[\frac{1}{2} - \frac{1}{2\pi}\arccos(\rho_{D\Sigma})]} \times \Phi[\delta_{11}(x-\mu_1) + \delta_{12}(y-\mu_2)]\Phi[\delta_{21}(x-\mu_1) + \delta_{22}(y-\mu_2)], \tag{5}$$

1-2. Simpkins

$$P(i,j) = \lambda \exp\left(-\frac{r_1^2 - 2wr_1r_2 + r_2^2}{2(1-w^2)}\right) \times \int_{-\infty}^{\alpha_1 r_1 + \alpha_2 r_2} \exp\left(-\frac{t^2}{2}\right) dt, \tag{6}$$

1-3. Skew-T

$$f(x_1,x_2;\alpha_1,\alpha_2,\rho,v) = 2t_2(x_1,x_2;\rho,v)T_1((\alpha_1x_1+\alpha_2x_2)\sqrt{\frac{v+2}{Q(x_1,x_2;\rho)+v}};v+2), \tag{7}$$

$$Q(x_1,x_2;\rho) = \frac{x_1^2 + x_2^2 - 2\rho x_1 x_2}{1-\rho^2}, \tag{8}$$

2. Inside-Skewness models

These methods make skewness inside of pdf. Contrary to outsid-skewness models, these models make changes in axis. Representatively, NSAS(Normalized sinh-arcsinh) model is a kind of inside-skewness models. It changes X's distribution inequally using inverse function with delta and epsilon.

In [3], two dimensional Gaussian kernels are used to model the asymmetric lens blur that has different amour of blur in radial and tangential directions. The skewness of blur kernels toward the radial direction is modeled with the skew-normal distribution in [9]. The parametric models have advantages over non-parametric models that an equation with a small number of parameters can characterize blur at any locations in a sensor. For applications such as deblurring [18], [19], [20], [21], parametric models provide blur kernels for each pixel efficiently.

C. Optical aberrations

In Optics, they say blur as aberration. In [26], Aberration PSF can be calculated as

$$I(r,\theta_i;z) = \frac{PS_p}{\pi^2\lambda^2 z^2} \mid \int_0^1 \int_0^{2\pi} exp[i\Phi(\rho,\theta)]exp[-\pi i\frac{R}{z}\rho r cos(\theta-\theta_i)]\rho d\rho d\theta \mid^2 \tag{9}$$

At this,a is the circular pupil of radius a and ρ is in units of a. ρ and θ consist spherical coordinate system. λ is a wavelength, R is the distance between the pupil plane and the image. Then, $\Phi(\rho,\theta)$ is the 'phase aberration'($\Phi = (2\pi/\lambda)W$) and W is the wave aberration. The phase aberration contains each aberrations' characteristics. P is the total power of light, and S_p is the area of pupil, S_p = πa^2. Finally, z means the focal length.

As mentioned, there are many kinds of aberrations in aberration researches[26],[28].

1. Spherical aberration

Spherical aberration is from area of aperture. Ideal camera has a dot aperture to filter out whole light without one direction-light. However, it is impossible, so more directions of light can pass through the aperture. Therefore, these many directions of light make shp shape on reception plane. This is the spherical aberration. This aberration is constant all over the image plane.

The spherical wave aberration is,

$$W(\rho,\theta) = A_s\rho^4 \tag{10}$$

and, $A_s \propto (aperture)^4$ spherical aberration is independent of the field of view(Fov).

2. Coma aberration

Coma is due to differences in magnification at different locations in a sensor. Real optical system is not perfect, any lens have identical magnification at each location. Therefore, there are skewed and triangular aberration on the receptive field.

The coma wave aberration is,

$$W(\rho,\theta) = A_c\rho^3 cos\theta \tag{11}$$

and, $A_c \propto (Fov), A_c \propto (aperture)^3$

3. Astigmatism aberration

Astigmatism is due to difference in focal points of meridional and sagittal rays. This is also from imperfection of lens. Each location of lens has different focal length, then these many characteristics of each location make complex aberration on the receptive field. Blur introduced by astigmatism is asymmetric in a sense blur is more severe in one direction than the other.

The astigmatism wave aberration is,

$$W(\rho,\theta) = A_a\rho^2 cos^2\theta \tag{12}$$

and, $A_a \propto (Fov)^4, A_a \propto (aperture)^2$

4. Defocus aberration

This aberration is from difference between focal length and distance between lens and object. Each sphere can focus on one dot at one distance(focal length), and focus on larger area at other distances. Therefore, the defocus aberration coefficient should be affected on object distance like this,

$$B_d = \pi N(\frac{R}{z} - 1) \tag{13}$$

In equation,$N = \frac{a^2}{\lambda R}$, a is the aperture value. Therefore, the defocus aberration is

$$\Phi(\rho,\theta) = \frac{2\pi}{\lambda}W(\rho,\theta) = B_d\rho^2 \tag{14}$$

5. Field Curvature aberration

The field curvature aberration is almost same with defocus aberration. The difference is that defocus aberration considers parallel planes, but field curvature is from spherical shape of lens and parallel shape of objects and sensor. This means that each location of lens has different distance with object. Therefore, each location should have identical defocus aberration, and it is said as field curvature aberration.

The field curvature wave aberration is

$$W(\rho,\theta) = A_d\rho^2 \tag{15}$$

and, $A_d \propto (Fov)^4, A_d \propto (aperture)^2$

6. Distortion aberration(Tilt aberration)

Images of a square grids passed through a lens is distorted. There are two types of distortion, one is the Pincusion distortion and the other one is the Barrel distortion. The Pincusion distortion make grids' edges cureved inside. Then, four vertex are on the outside from center points, so two edges meet at a vertex with sharpness. Otherwise, the Barrel distortion makes square grids as circle. Each edge is curved outside from center. These distortions make aberrations.

The distortion wave aberration is

$$W(\rho,\theta) = A_t\rho cos\theta \tag{16}$$

and, $A_t \propto (Fov)^3, A_t \propto (aperture)$

The process of aberration formation can be analyzed to model the lens blur. In [10], the effect of a lens is modeled by a mapping of incident rays to a plane. With specifications of a lens system, the psf's at any locations in a sensor can be found from a composite mapping that models all the effects of the entire lens in a system. The effect of the aberration formation to a photographed image is found by ray tracing. In [11], a polynomial model is used to model the aberration of a lens. Model parameters are estimated by fitting a polynomial model to a photographed test pattern. With the estimated parameters, psf's are found by ray counting integrals. These approaches have advantages that physically possible blur kernels can be found. However, the psf's are found via methods that require significant amount of computations such as ray tracing or ray counting integrals. For applications that require efficient computations of psf's at various pixel locations, the computational complexity may be too high.

This paper presents parametric models to accurately model the non-stationary asymmetric lens blur. Similar to models in [3], [9], the proposed models are parametric models that provide efficient method to characterize the blur at any pixel locations in a sensor with an equation with a set of parameters. The NSAS and NEAS models includes the Gaussian model used in [3]. The NSAS is similar to the skew-normal model [9] in addressing the asymmetry and the skewness of lens blur. Statistical properties of the NSAS and skew-normal distributions can be found in [15]. For modeling of lens blur, the two distributions provide different shapes of skewness. The NSAS model has an advantage that it has specific parameters to control the skewness and the kurtosis. The shapes of the two dimensional kernels are different than the ones of skew-normal distribution. Moreover, the NSAS model can be easily generalized to the NEAS model to provide more flexible shapes of blur kernels than the skew-normal distributions.

III. Contents

A. Asymmetric Blur Model

Blur that is asymmetric in the two principal directions can be modeled by the two dimensional Gaussian distribution [3]. The blur kernel of the Gaussian model is given by

$$h(i,j) = c \exp\left(-\frac{1}{2}\mathbf{x}^{\mathrm{T}}\mathbf{R}^{-1}\mathbf{x}\right), \tag{17}$$

where c is a normalization constant, $\mathbf{x} = [i,j]^{\mathrm{T}}$, and $\mathbf{R}$ is the covariance matrix. With different choices of the covariance matrices, the principal directions of the kernels can be rotated, and the spreads of the kernels in the two principal directions can be adjusted separately. The Gaussian model can model the lens blur asymmetric in the radial and tangential directions with blur kernels with rotated elliptic contours. However, the skewness in the radial direction cannot be modeled by the Gaussian model.

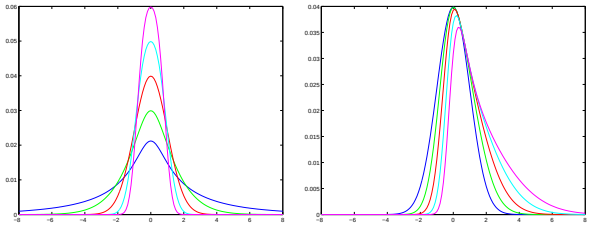

(a) (b)

Fig. 2. Examples of the NSAS distribution function, (a) δ = 0.5, 0.75, 1, 1.25, 1.5, $\epsilon = 0$, and (b) $\delta = 1$, ϵ = 0, -0.25, -0.5, -0.75, -1, in the order of blue, green, red, cyan, magenta.

Skew-normal distribution is a Gaussian-like distribution used in statistics to model distribution with skewness [12]. Two dimensional skew-normal distribution is used to model non-stationary asymmetric lens blur in [9]. The blur kernels can have Gaussian-like shapes with rotation and skewness into one chosen direction.

Normal sinh-arcsinh (NSAS) distribution is a Gaussian-like distribution also used in statistics to model distributions with skewness [13], [14], [15]. The one dimensional NSAS distribution is given by

$$f(x) = c\frac{C(x)}{\sqrt{1+x^2}} \exp\left(-\frac{1}{2}S^2(x)\right), \tag{18}$$

where

$$\begin{aligned} S(x) &= \sinh(\delta \text{arcsinh}(x) + \epsilon) \\ C(x) &= \delta \cosh(\delta \text{arcsinh}(x) + \epsilon). \end{aligned} \tag{19}$$

and c is the normalization constant. The parameters δ and ϵ controls the spread and skewness of the distribution, respectively. Fig. 2 shows how the parameters change the shape of the NSAS distribution function.

Fig. 2 (a) shows examples of the NSAS distributions at $\delta = 0.5, 0.75, 1, 1.25, 1.5$ and $\epsilon = 0$. The spread of the NSAS distribution increases with smaller values of δ. Fig. 2 (b) shows examples of the NSAS distributions at $\delta = 1$ and $\epsilon = 0, -0.25, -0.5, -0.75, -1$. The distribution shows larger skewness with smaller values of ϵ.

In this work, two dimensional NSAS distribution is used to model lens blur with more complicated shapes. Two dimensional blur kernel is given by

$$h(i,j) = c\frac{C_1(i')}{\sqrt{1+i'^2}}\frac{C_2(j')}{\sqrt{1+j'^2}} \exp\left(-\frac{1}{2}\mathbf{x}^{\mathrm{T}}\mathbf{x}\right), \tag{20}$$

where

$$\mathbf{x} = \begin{bmatrix} S_1(i') \\ S_2(j') \end{bmatrix} \tag{21}$$

and

$$\begin{aligned} S_n(k) &= \sinh(\delta_n \text{arcsinh}(k) + \epsilon_n) \\ C_n(k) &= \delta_n \cosh(\delta_n \text{arcsinh}(k) + \epsilon_n) \end{aligned} \tag{22}$$

for $n \in \{1, 2\}$. The kernel is rotated, sheared, scaled, and shifted by

$$\begin{bmatrix} i' \\ j' \end{bmatrix} = \mathbf{T} \begin{bmatrix} i \\ j \end{bmatrix} - \begin{bmatrix} \mu_1 \\ \mu_2 \end{bmatrix}, \tag{23}$$

where the affine transform $\mathbf{T}$ is given by

$$\mathbf{T} = \begin{bmatrix} 1/\sigma_1 & 0 \\ 0 & 1/\sigma_2 \end{bmatrix} \begin{bmatrix} 1 + b_1 b_2 & b_2 \\ b_1 & 1 \end{bmatrix} \begin{bmatrix} \cos\theta & \sin\theta \\ -\sin\theta & \cos\theta \end{bmatrix}. \tag{24}$$

This model is denoted by the NSAS model.

There are four parameters, δ's and ϵ's in (22), that control the spread and skewness of the kernel. There are seven parameters involved in the affine transform and the shift of the two independent variables i and j. The parameters μ_1 and μ_2 control the location of the kernel in vertical and horizontal directions, respectively. The parameter θ rotates the two directions. The parameters b_1 and b_2 introduce shear of the two directions. The parameters σ_1 and σ_2 control the spread of the kernel in the rotated and sheared directions.

The NSAS model is further generalized by separating δ's and ϵ's for the two exponential functions in the $\sinh$ function. In particular, $S_n(k)$ and $C_n(k)$ in the model are generalized by

$$\begin{aligned} S_n(k) &= \Big(\exp(\ \ \delta_n^l \text{arcsinh}(k) + \epsilon_n^l) \\ &- \ \ \exp(-\delta_n^r \text{arcsinh}(k) - \epsilon_n^r)\Big)/2 \\ C_n(k) &= \Big(\delta_n^l \exp(\ \ \delta_n^l \text{arcsinh}(k) + \epsilon_n^l) \\ &+ \ \ \delta_n^r \exp(-\delta_n^r \text{arcsinh}(k) - \epsilon_n^r)\Big)/2 \end{aligned} \tag{25}$$

for $n \in \{1, 2\}$. The model is named as the normal exponential-arcsinh (NEAS) model. There are eight parameters, δ's and ϵ's in (25), that control the spread and skewness of the kernel. There are seven parameters involved in the affine transform and the shift.

The NEAS model includes the NSAS model. One can reduce the NEAS model to the NSAS model by setting $\delta_n^l = \delta_n^r$ and $\epsilon_n^l = \epsilon_n^r$ for $n = 1, 2$. The NSAS model includes the Gaussian model. One can reduce the NSAS model to the Gaussian model by setting $\delta = 1$ and $\epsilon = 0$. The NSAS and NEAS models are generalization of the Gaussian model to accommodate more and more flexible shapes of kernels.

Fig. 3 shows examples of the two dimensional NSAS and NEAS blur kernels with different parameters The parameters to generate the blur kernels are given in Table I. The parameters that

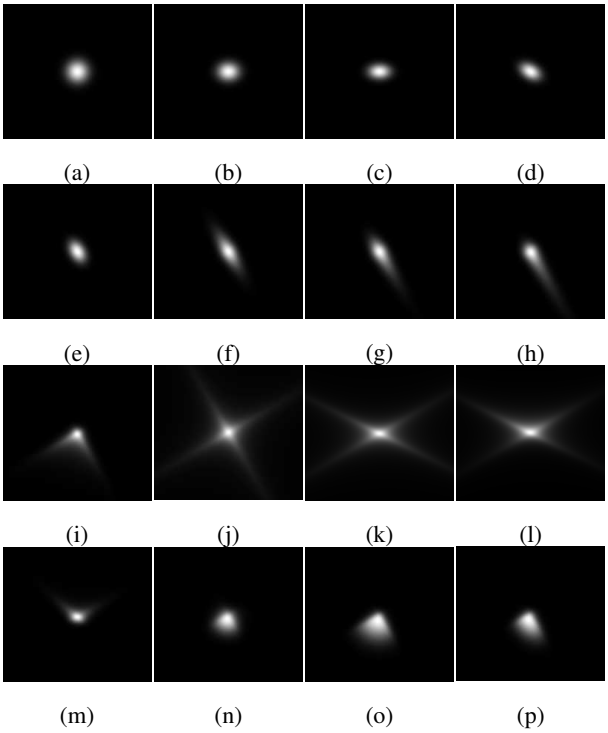

Fig. 3. Examples of kernel shapes of the NSAS and NEAS models at different parameters.

are changed from the previous examples are shown in boldface. Fig. 3 (a), (b), and (c) show the effect of σ_2 that changes the spread of kernel in the horizontal direction. The effect of the σ_1 is the same but in the other direction. Fig. 3 (d) and (e) shows the rotation of the kernel with θ. Fig. 3 (f) shows the effect of δ_1 that controls the spread of the kernel in one of the principal directions. The effect of the σ and δ are similar in a sense that both control the spread of the kernels. Both parameters are kept in the model so that when δ's are one and ϵ's are zero we have a simple quadratic exponent term. Fig. 3 (g) and (h) show the effect of ϵ_1's that control the skewness of kernel. As ϵ_1 increases, the kernels have longer tails in one side of a principal direction, turning into comet-like shapes. The kernels in Fig 3 (i) and (j) have different values of σ, δ, and ϵ, showing kernels with two and four long tails, respectively. Fig. 3 (k) shows the effect of b_1 that controls the shear of two principal directions. With different combinations of δ_1^l, δ_2^r, and δ_2^l, δ_2^r, kernels can have different tails in each side of the principal directions as shown in Fig. 3 (l) and (m). The increases in the ϵ's with different values of δ_1^l, δ_2^r, and δ_2^l, δ_2^r provide clamshell-like kernels in Fig. 3 (n), (o) and (p). The different combinations of ϵ_2^l and ϵ_2^r makes the clamshell longer in one direction. The NSAS and NEAS models can provide blur kernels with many different types of contours with asymmetry and skewness. In particular, the comet-shape and clamshell-shape kernels are suitable for modeling the lens blur that show radial-tangential and inward-outward radial asymmetry. Note that the kernels in Fig. 3 (a) to (e) are Gaussian, which is included in the NSAS and NEAS models.

TABLE I

PARAMETERS OF THE NSAS AND NEAS MODELS USED FOR KERNELS IN FIG. 3

	θ	b_1	b_2	σ_1	σ_2	m_1	m_2	δ_1^l	δ_2^r	δ_2^l	δ_2^r	ϵ_1^l	ϵ_1^r	ϵ_2^l	ϵ_2^r
(a)	0	0	0	1	1	0	0	1	1	1	1	0	0	0	0
(b)	0	0	0	1	**5/6**	0	0	1	1	1	1	0	0	0	0
(c)	0	0	0	1	**2/3**	0	0	1	1	1	1	0	0	0	0
(d)	**$\pi/6$**	0	0	1	2/3	0	0	1	1	1	1	0	0	0	0
(e)	**$\pi/3$**	0	0	1	2/3	0	0	1	1	1	1	0	0	0	0
(f)	$\pi/3$	0	0	1	2/3	0	0	**2/3**	**2/3**	1	1	0	0	0	0
(g)	$\pi/3$	0	0	1	2/3	0	0	2/3	2/3	1	1	**1/3**	**1/3**	0	0
(h)	$\pi/3$	0	0	1	2/3	0	0	2/3	2/3	1	1	**2/3**	**2/3**	0	0
(i)	$\pi/3$	0	0	**2/3**	2/3	0	0	2/3	2/3	**2/3**	**2/3**	2/3	2/3	**2/3**	**2/3**
(j)	$\pi/3$	0	0	2/3	2/3	0	0	**1/5**	**1/5**	**1/5**	**1/5**	**0**	**0**	**0**	**0**
(k)	$\pi/3$	**2/3**	0	2/3	2/3	0	0	1/5	1/5	1/5	1/5	0	0	0	0
(l)	$\pi/3$	2/3	0	2/3	2/3	0	0	1/5	**2/5**	1/5	**2/5**	0	0	0	0
(m)	$\pi/3$	2/3	0	2/3	2/3	0	0	**1**	**1/2**	**1**	**1/2**	0	0	0	0
(n)	$\pi/3$	**0**	0	2/3	2/3	0	0	1	1/2	1	1/2	**2/3**	**2/3**	**2/3**	**2/3**
(o)	$\pi/3$	0	0	2/3	2/3	0	0	1	1/2	1	1/2	**1**	**1**	**1**	**1**
(p)	$\pi/3$	0	0	2/3	2/3	0	0	1	1/2	1	1/2	1	1	**2/3**	1

B. Asymmetric Blur Estimation

Blur of a lens is estimated using a test image captured with a set of lenses at various aperture following the procedure outlined in [3]. First, a non-parametric blur kernel is estimated by minimizing the difference between the photographed image and the image blurred by a non-parametric kernel. Then, the parametric blur kernel is estimated by minimizing the difference between the non-parametric and parametric kernels. This two-step approach is computationally fast and works without regularization on the shape of the blur kernel [3].

Images are captured with a camera parallel to the images and focused at the center of the images. The camera is on a tripod, and the shutter is released remotely to reduce vibration. The ISO is set to the lowest value to reduce the noise in the image. The image is captured in the raw format and converted with a software. Two test images are used: an image with repeating blocks of white circular patterns on black background and a random noise image. The Fig. 4 shows examples of the test images. Blocks are indicated by the four red markers at the four corners.

Blur inside each block of the captured image is estimated separately. The corners of a block are found by locating the four red markers, and the block of a captured image is extracted. A homography transform [22] is applied to transform the extracted block of image into a rectangle shape whose size is the same as the one block of the test pattern. The dynamic range is normalized so that the white

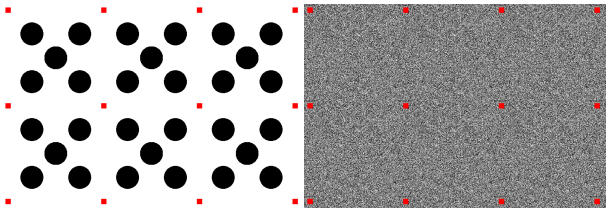

(a) (b)

Fig. 4. Example of the test image for blur estimation, (a) test pattern and (b) random noise pattern

and black regions have the same grayscale values as the test pattern. The blur is estimated comparing the homography transformed and dynamic range compensated observed image to the mathematical definition of the test pattern.

Blur is assumed to be space-invariant inside a given block. The observed image g is obtained by a convolution of the non-parametric blur kernel h_{np} and the test pattern f by

$$g(i,j) = \sum_{s,t} f(i-s, j-t) h_{np}(s,t). \tag{26}$$

Non-parametric blur kernels are found following the method in [3] by solving the following optimization problem

$$\underset{\mathbf{h}_{\mathrm{np}}}{\text{minimize}} \ \|\mathbf{g} - \mathbf{F}\mathbf{h}_{\mathrm{np}}\|^2 \tag{27}$$

where $\mathbf{g}$ and $\mathbf{h}_{np}$ are the lexicographically ordered observed image and the non-parametric blur kernel, respectively. The elements of the matrix $\mathbf{F}$ are the pixel values in f arranged to represent the convolution in (26). Non-parametric blur kernels are also found following the method in [7] by

$$\mathcal{H}_{np}(u,v) = \mathcal{G}(u,v)/\mathcal{F}(u,v), \tag{28}$$

where $\mathcal{H}_{np}, \mathcal{G}(u,v)$ and $\mathcal{F}(u,v)$ are the discrete Fourier transforms of h_{np}, g, and f. In both methods, non-parametric blur kernels are post-processed with thresholding and re-normalization such that all the values are positive and small values due to noise are removed.

A parametric blur kernel is estimated by minimizing the difference between the non-parametric and parametric kernels by

$$\underset{\mathbf{p}}{\text{minimize}} \ \|\mathbf{h}_{\mathrm{np}} - \mathbf{h}(\mathbf{p})\|^2 \tag{29}$$

where $\mathbf{h}(\mathbf{p})$ is the lexicographically ordered parametric blur kernel and $\mathbf{p}$ represents the parameters of a model. The parametric blur kernel is post-processed with thresholding and re-normalization. The parameter of the NSAS model is

$$\mathbf{p} = [\delta_1, \delta_2, \epsilon_1, \epsilon_2, \Theta] \tag{30}$$

and the parameters of the NEAS model is

$$\mathbf{p} = [\delta_1^l, \delta_2^r, \delta_2^l, \delta_2^r, \epsilon_1^l, \epsilon_1^r, \epsilon_2^l, \epsilon_2^r, \Theta] \tag{31}$$

where $\Theta = [\theta, b_1, b_2, \sigma_1, \sigma_2, \mu_1, \mu_2]$ is the parameters for the affine transform with the shift.

IV. Experiments and Discussion

A. Asymmetric Blur Model

The blur of a set of single focal length lenses are estimated. The lenses used in the experiments are 35mm, 50mm, 105mm, and 135mm with the maximum aperture of f/1.8, f/1.8, f/2.8, and f/2.0, respectively. A camera equipped with a 12 mega pixel full frame sensor with the minimum ISO of 200 is used. The test image used in the blur estimation consists of blocks of repeating patterns. 16×25, 19×28, 19×29, and 16×25 blocks of repeating patterns are used for 35mm, 50mm, 105mm, and 135mm lenses. Each block of pattern is 256×256 pixels. The test image is photographed, and the blocks that contain one test pattern are extracted. Each block is transformed into rectangle shape images of 256×256 pixels by a homography transform. The dynamic range of the homographs transformed block is modified to match the dynamic range of the test pattern with black at 16 and white at 238 in 8 bit grayscale. The blur kernel of the size 21×21 is estimated. The support of the kernel is set such that $h(i, j) = 0$ for $|i| > 10$ or $|j| > 10$. The constant c normalizes the kernel such that the sum of elements is one. For optimization, Levenberg-Marquardt algorithm [23] is used. In order to ensure the algorithm finds the optimal parameters, the optimization routines are started with random initial solutions, exept for θ which is initialized based on the geometry, several times and the best case parameters are selected.

Fig. 5 shows the estimated non-parametric kernels estimated for the 16×25 blocks. The 35mm f/1.8 lens at aperture of f/2.0 is used in the experiment. The estimated blur kernels show rotation of the principal directions depending on the locations of blocks. The estimated blur show asymmetry in a sense that the blur is more severe in radial direction than in tangential direction, and also in a sense blur is skewed in the radial direction. The characteristics of the estimated non-parametric blur is consistent with the non-parametric blur estimation reported in [3], [9].

Fig. 6 shows example of blur kernels estimated using the Gaussian, skew-normal, NSAS, and NEAS models for the locations of (a) cyan and (b) yellow squares in Fig. 5, respectively. The kernels are interpolated for smoother presentation. Both kernel shapes and their contours are shown. Blur

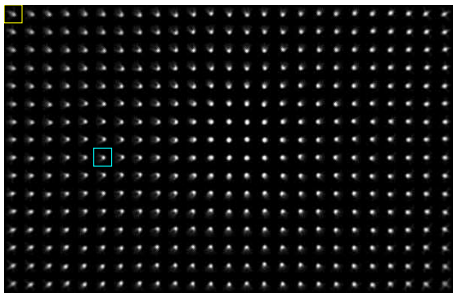

Fig. 5. 16×25 block-wise non-parametric estimation of blur kernels of a 35mm f/1.8 lens at aperture f/2.0.

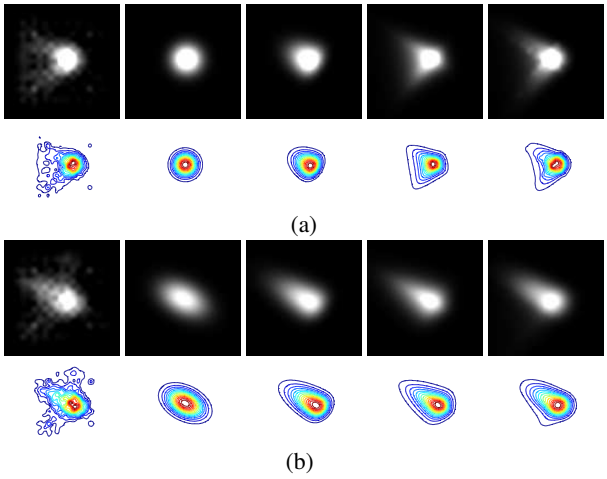

Fig. 6. Blur kernels of a 35mm lens at aperture f/2.0 at locations of (a) cyan square and (b) yellow square in Fig. 5. The kernels and their contours are shown. from left to right: non-parametric, Gaussian, skew-normal, NSAS, and NEAS models.

asymmetric in radial and tangential directions is modeled by all the models. However, blur skewed in the radial directions can be modeled by the skew-normal, NSAS and NEAS models but not by the Gaussian model. It can be seen that the NSAS and NEAS model are more flexible than the Gaussian and skew-normal models in modeling blur with complicated contours. For example, non-parametric blur kernel in Fig. 6 (a) has two tails in the separate directions. This shape can be modeled by the NSAS and NEAS models, but not by the skew-normal model.

Table II shows the mean square error (MSE) between the parametric kernels and the non-parametric blur kernels. The non-parametric kernels are obtained using a test pattern in Fig. 4 (a) using the optimization given in (27). The results for the four single focal length lenses are shown. For comparison, the Gaussian model and the skew-normal model in [9] are included. We also implement two additional distributions, the skew-normal distribution [12] and the skew-T distribution [16], that are used in statistics to model distributions with skewness. Usually photographs taken with the aperture stop down to f/16 show sharp images across the entire frame. The sharpness at the corners of photographs

TABLE II

MSE BETWEEN THE PARAMETRIC KERNELS AND NON-PARAMETRIC KERNELS ESTIMATED USING A TEST PATTERN

	aperture	Gaussian	skew-normal [9]	skew-normal [12]	Skew-T	NSAS	NEAS
35mm	f/1.8	0.000965	0.000773	0.000698	0.000834	0.000620	0.000565
	f/4	0.000339	0.000332	0.000326	0.000346	0.000319	0.000311
	f/8	0.000314	0.000307	0.000301	0.000316	0.000284	0.000279
	f/16	0.000198	0.000191	0.000184	0.000188	0.000181	0.000177
50mm	f/1.8	0.001553	0.001399	0.001261	0.001502	0.001269	0.001220
	f/4	0.000752	0.000672	0.000668	0.000725	0.000632	0.000602
	f/8	0.000883	0.000880	0.000879	0.000937	0.000769	0.000755
	f/16	0.001075	0.001074	0.001106	0.001127	0.000883	0.000870
105mm	f/2.8	0.000415	0.000411	0.000447	0.000459	0.000371	0.000361
	f/4	0.000507	0.000503	0.000500	0.000563	0.000452	0.000439
	f/8	0.000377	0.000364	0.000363	0.000375	0.000299	0.000289
	f/16	0.000729	0.000727	0.000726	0.000759	0.000656	0.000642
135mm	f/4	0.000561	0.000393	0.000398	0.000379	0.000355	0.000320
	f/8	0.000848	0.000828	0.000899	0.000809	0.000753	0.000739
	f/16	0.000741	0.000738	0.000735	0.000779	0.000677	0.000663

TABLE III

MSE BETWEEN THE PARAMETRIC KERNELS AND NON-PARAMETRIC KERNELS ESTIMATED USING A RANDOM NOISE PATTERN

	aperture	Gaussian	skew-normal [9]	skew-normal [12]	Skew-T	NSAS	NEAS
50mm	f/1.8	0.006775	0.004585	0.003259	0.003470	0.002994	0.002204
	f/16	0.003271	0.003230	0.003210	0.003236	0.003080	0.002764
105mm	f/2.8	0.002610	0.00257	0.002552	0.002522	0.002338	0.002072
	f/16	0.002153	0.00213	0.002130	0.002126	0.001991	0.001753

starts to deteriorate as the aperture opens up to the maximum aperture. The MSE's at wider aperture are bigger for all the models than those at smaller aperture. For small aperture, for example f/16, the models do not show considerable differences, even though the MSE's are always bigger in the order of Gaussian, skew-normal, skew-T, NSAS, and NEAS models. However, for wider aperture,

TABLE IV

MSE BETWEEN THE PARAMETRIC KERNELS AND MEASURED NON-PARAMETRIC BLUR KERNELS FROM [8]

	aperture	Gaussian	skew-normal [9]	skew-normal [12]	Skew-T	NSAS	NEAS
N/A	N/A	3.69E-05	2.61E-05	1.90E-05	9.45E-06	1.58E-05	8.96E-06

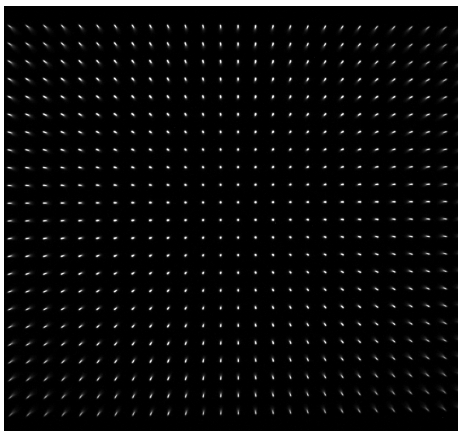

Fig. 7. Blur kernels provided by [8].

for example f/1.8, f/2.0, f/2.8, and f/4 depending on the lens, the differences in MSE's between the models become noticeable. As can be seen in Fig. 5, the blur becomes not only more severe but also more complicated at the corners of the sensor frame when the aperture is wide open. The Gaussian model fails to portrait the complicated asymmetric nature of the lens blur. The models that can address the asymmetry and the skewness of the blur kernels provide smaller MSE's. It can be seen that the NSAS model provides smaller MSE's than the skew-normal and skew-T models. The NEAS model can provide the most complicated shapes of blur kernels among the models. The MSE's of the NEAS model are smaller than all the other models that address the asymmetry and the skewness.

Table III shows the MSE's between the parametric kernels and the non-parametric blur kernels. This time, the non-parametric kernels are obtained using a random noise pattern in Fig. 4 (b) using the DFT given in (28). The results for the two single focal length lenses are shown. The MSE results show the similar trends as the results in Table II. The models that can address the asymmetry and the skewness provide better MSE than the Gaussian model. The most flexible NEAS model provides the lowest MSE's. We repeated the experiments to show that the accuracy of the models are not affected by the estimation method used to find the non-parametric blur kernels. We also measure the difference between the parametric kernels obtained with the optimization method in (27) and with the DFT method in (28) using the random noise pattern. Average MSE between the two non-parametric kernels is 0.0042, average correlation is 0.9427, and average Bhattacharyya distance is 0.0098. The differences between the kernels obtained by the two estimation methods are small.

Table IV shows the MSE's between the parametric kernels and the non-parametric blur kernels from the database of blur kernels provided by [8]. The blur kernels, shown in Fig. 7, are obtained by photographing a test pattern consists of grids of point sources. The results are consistent with the results in Table II and III.

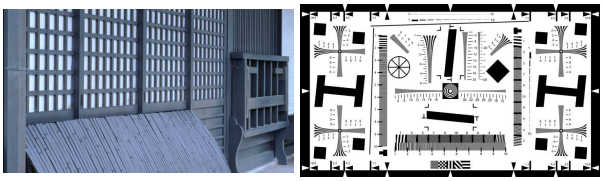

(a) (b)

Fig. 8. Test images used in the SSIM experiment, (a) photographic image and (b) test pattern.

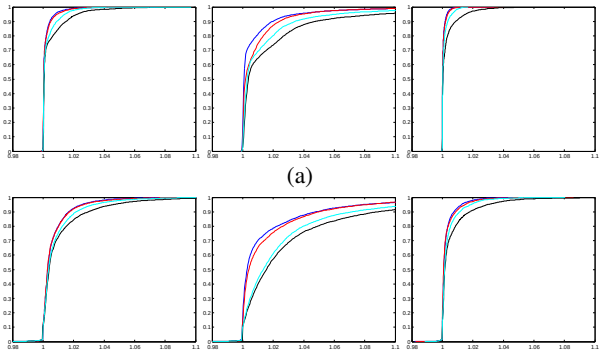

(a)

(b)

Fig. 9. CDF of SSIM error ratios at all the aperture values, left: 35mm, center: 50mm, right 135mm, (a) with blocks of a photographic image, (b) with blocks of a test pattern. black: Gaussian, cyan: skew-normal, red: NSAS, blue: NEAS

B. Deblur with Asymmetric Blur Model

In order to quantify the advantages of using the NSAS and NEAS models over the other models, experiments outlined in [3] are performed. Blocks of a natural photograph and a test pattern, shown in Fig. 8, are blurred by the non-parametric kernels. Blurred images are deblurred using the non-parametric blur kernel and corresponding parametric blur kernels. The visual quality of deblurred images is measured by the mean structural similarity index (SSIM) [24] between the deblurred and original images. The error ratios between the SSIM obtained using the non-parametric and parametric models

$$r_{\text{model}} = \frac{\text{SSIM}_{\text{np}} + 2}{\text{SSIM}_{\text{model}} + 2}, \tag{32}$$

are measured. Blur kernels estimated for all the blocks at various aperture using the non-parametric, Gaussian, skew-normal, NSAS, and NEAS models are used in the experiment. An augmented Lagrangian based deblurring algorithm given in [25] is used for deblurring. 35mm and 50mm lenses at aperture values $\{1.8, 4, 8, 16\}$ and a 135mm lens at aperture values $\{4, 8, 16\}$ are used.

Fig. 9 shows the cumulative distribution functions (cdf's) of the error ratios. The cdf's of error ratios collected at all the aperture are shown. Fig. 9 (a) shows the results obtained with a natural photograph, and (b) shows the results obtained with a test pattern. It can be seen that the NSAS

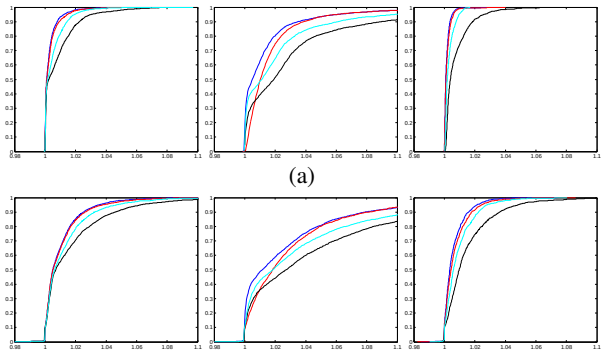

Fig. 10. CDF of SSIM error ratios at aperture values wider than f/4, left: 35mm, center: 50mm, right 135mm, (a) with blocks of a photographic image, (b) with blocks of a test pattern. black: Gaussian, cyan: skew-normal, red: NSAS, blue: NEAS

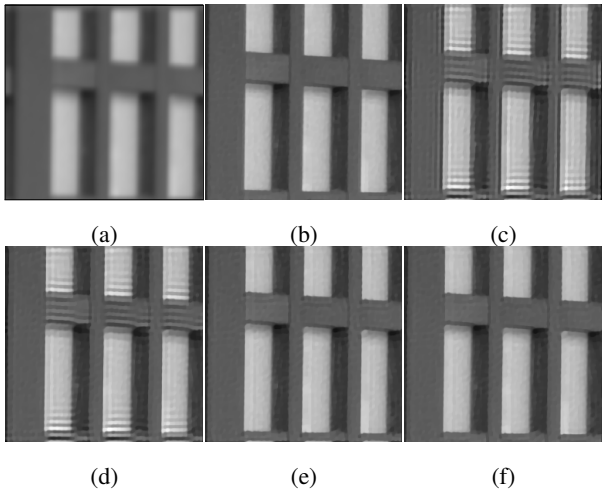

Fig. 11. Example of deblurred images in the SSIM experiment, (a) image blurred by non-parametric kernel, deblurred images using (b) non-parametric, (c) Gaussian, (d) skew-normal (e) NSAS, and (f) NEAS models.

and NEAS models provide smaller error ratios than the Gaussian and the skew-normal models. The improvement is slightly better with the NEAS model than with the NSAS model.

Fig. 10 shows the cdf's of the error ratios collected for aperture values wider than f/4. Fig. 9 (a) shows the results obtained with a natural photograph, and (b) shows the results obtained with a test pattern. The advantage of using the NSAS and NEAS model over the Gaussian model is easier to notice at wider aperture, for which softness at the corners of a sensor frame is more apparent.

A block of images in the evaluation of SSIM experiments for which the proposed models show biggest differences in SSIM is shown in Fig. 11. An image blurred by the non-parametric blur kernel is shown in Fig. 11 (a). An image deblurred by the same non-parametric blur kernel is shown in Fig. 11 (b). It can be seen that when the image is deblurred using the correct blur kernel, an

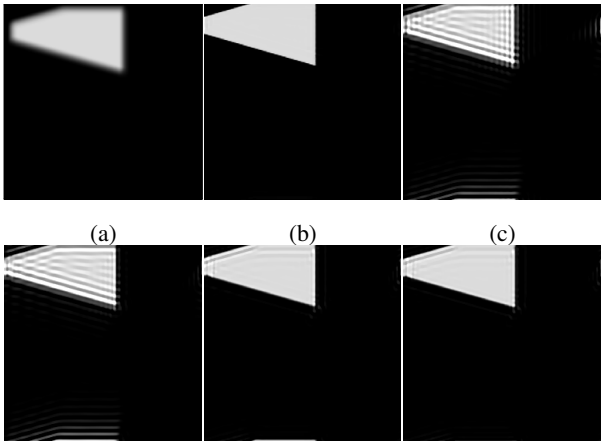

Fig. 12. Example of deblurred images in the SSIM experiment, (a) image blurred by non-parametric kernel, deblurred images using (b) non-parametric, (c) Gaussian, (d) skew-normal (e) NSAS, and (f) NEAS models.

image close to the original can be restored by deblurring. Deblurred images using the Gaussian, skew-normal, NSAS, and NEAS kernels are shown in Fig. 11 (c), (d), (e), and (f), respectively. Mismatches between the blur kernels used in the blur and deblur processes degrade the quality of the deblurred images. The SSIM values are 0.97, 0.65, 0.79, 0.92, 0.94 for the images deblurred by the non-parametric, Gaussian, skew-normal, NSAS, and NEAS models, respectively. The NSAS and NEAS models provide deblurred images of higher quality with less ring near major edges of the door frames. Also, blocks of synthetic image used in SSIM comparison are shown in Fig. 12.

Fig. 13 and 14 show deblurring of photographs taken with 35mm f/1.8 and 50mm f/1.8 lenses, respectively, at the maximum aperture. Regularized inverse is applied block-wise for the deblurring, with blur kernels characterized block-wisely using the non-parametric, Gaussian, skew-normal, NSAS, and NEAS models. Regularization parameters are experimentally found. The same regularization parameter is used for all the models. The original images are shown in (a). Parts of the images in the red, yellow, and cyan boxes are shown in (c). Parts of the images deblurred using the Gaussian, skew-normal, NSAS, and NEAS models are shown in (d), (e), (f), and (g), respectively. The blur kernels at the locations of the boxes are shown in (b). The leftmost column shows the non-parametric blur kernels. The rest of blur kernels are for the images in the same locations of image in the figures (d) to (g). It can be seen that the NSAS and NEAS models provides blur kernels closer to the non-parametric kernels. In the images deblurred using the Gaussian and skew-normal models, shown in (d) and (e), respectively, there are visible ringing near major edges. The ringing is considerably less in the images deblurred using the NSAS and NEAS models, shown in (f) and (g), respectively. The results with photographed images are consistent with the results in the SSIM experiments. Mismatches between the blur introduced by a lens and the blur used in the deblurring process causing ringing

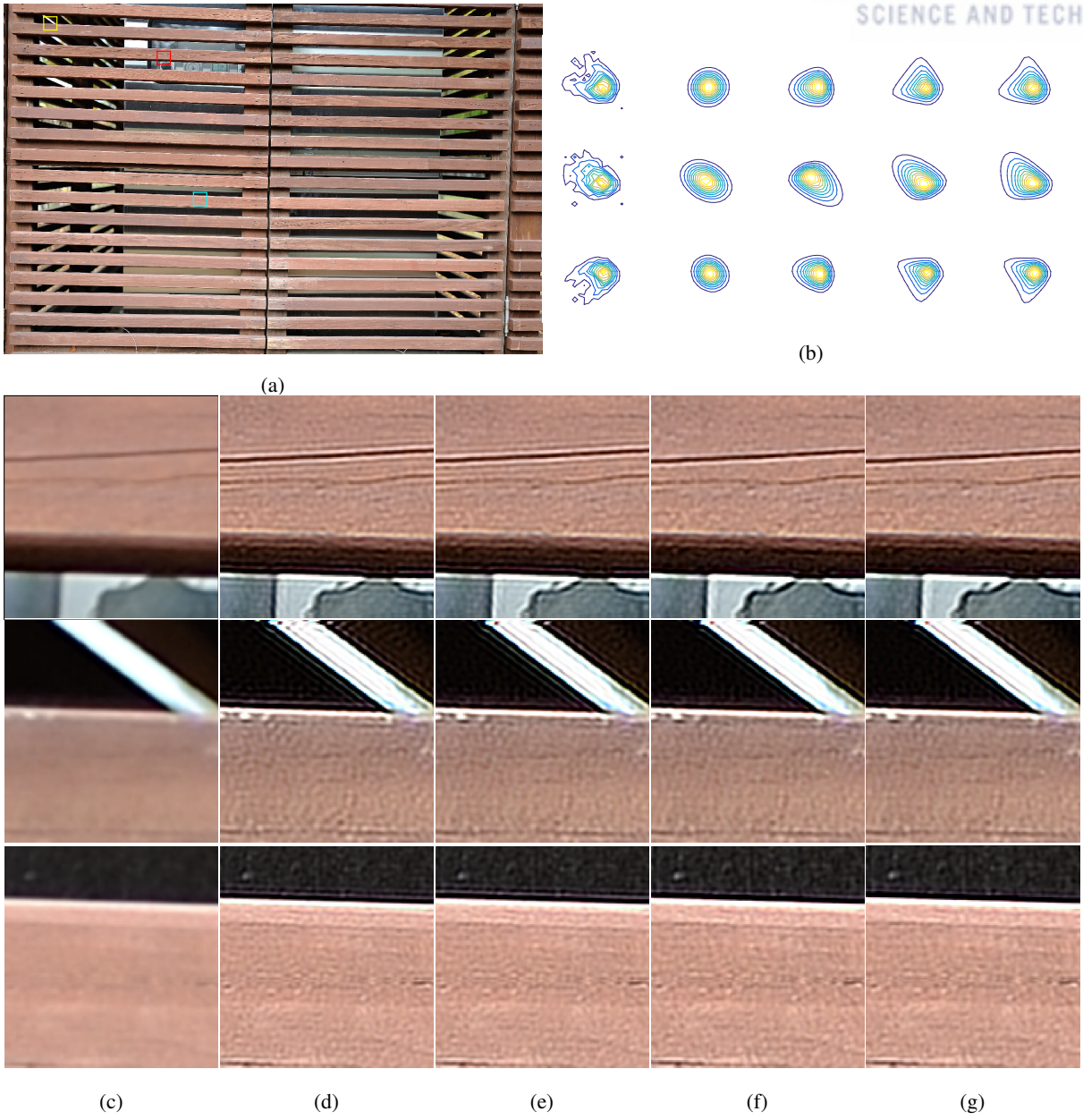

(a) (b) (c) (d) (e) (f) (g)

Fig. 13. Example of deblurred image with 35mm f/1.8 lens at aperture f/1.8, (a) original photo, (b) coutour plots of non-parametric and parametric psf's for images in (d) to (g), (c) parts of original images, parts of deblurred images using (d) non-parametric, (e) Gaussian, (f) skew-normal, (h) NSAS, and (g) NEAS models. Parts of the images are from top: red, middle: yellow, and bottom: cyan boxes of (a).

near major edges. The NSAS and NEAS models provide more flexible shapes of blur kernels for accurate modeling of non-stationary asymmetric lens blur, and deblurred images show less visible ringing near major edges.

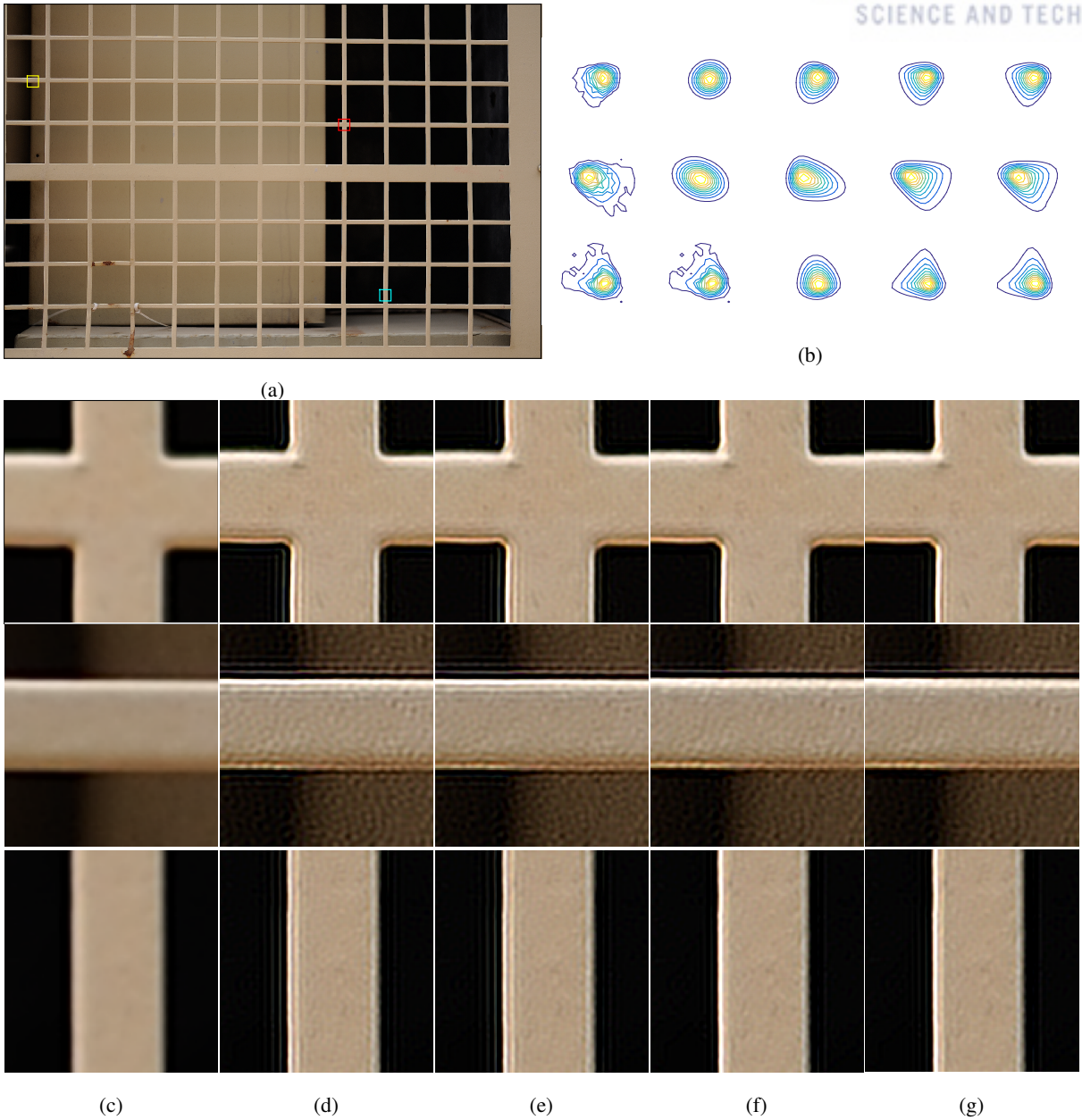

Fig. 14. Example of deblurred image with 50mm f/1.8 lens at aperture f/1.8, (a) original photo, (b) coutour plots of non-parametric and parametric psf's for images in (d) to (g), (c) parts of original images, parts of deblurred images using (d) non-parametric, (e) Gaussian, (f) skew-normal, (h) NSAS, and (g) NEAS models. Parts of the images are from top: red, middle: yellow, and bottom: cyan boxes of (a).

V. Conclusion

This paper presents parametric blur models based on the two dimensional NSAS distribution. The proposed models provide blur kernels flexible enough to model complicated shapes of lens blur with asymmetry and skewness, such as clam shell like blurs or blurs with two tails in separate directions. In terms of modeling accuracy, the proposed models provide significant improvement over the Gaussian model and noticeable improvement over the other models that addresses the asymmetry

and skewness. Furthermore, other skew models can make only skewness, they cannot make tails. From these differences, NSAS and NEAS are much accurate and more suitable to model real PSFs. In terms of deblurring performance, the images deblurred using the proposed models show less ringing near major edges. The NSAS and NEAS models can be used in applications that require accurate and efficient computation of non-stationary asymmetric lens blur at any pixel locations.

REFERENCES

[1] W. J. Smith, “Modern Optical Engineering”, 2nd ed. McGraw-Hill, New York, 1990.

[2] Zemax, *Zebase, Optical Design Database*, Version 5.0, San Diego: Zemax Development Corp, 2003.

[3] E. Kee, S. Paris, S. Chen, and J. Wang, “Modeling and removing spatially varying optical blur”, *Proceedings of the IEEE Conf. on Computational Photography*, pp. 1-8, 2011.

[4] F. Heide, M. Rouf, M. B. Hullin, B. Labitzke, W. Heidrich, and A. Kolb, “High-quality computational imaging through simple lenses”, *ACM Trans. Graph*, Vol. 32, Iss. 5, 2013.

[5] C. J. Schuler, M. Hirsch, S. Harmeling, and B. Scholkepf, “Non-stationary correction of optical aberrations”, *IEEE International Conference on Computer Vision*, pp. 659-666, 2011.

[6] N. Joshi, R. Szeliski, and D. Kriegman, “PSF estimation using sharp edge prediction”, *IEEE Conf. Computer Vision and Pattern Recognition*, pp. 1-8, 2008.

[7] J. Brauers, C. Seiler, and T. Aach,“Direct PSF estimation using a random noise target, *Proc. SPIE* 7537, 75370B, 2010.

[8] P. Rangarajan, Private communication, 2015.

[9] J. Simpkins and R. L. Stevenson, “Parameterized modeling of spatially varying optical blur”, *J. Electron. Imaging* 23(1), 013005, 2014.

[10] M. B. Hullin, J. Hanika, and W. Heidrich, “Polynomial optics:a construction kit for efficient ray-tracing of lens systems”, *Eurographics Symposium on Rendering* 31(4), 2012.

[11] H. Tang and K. N. Kutulakos, “What Does an Aberrated Photo Tell Us about the Lens and the Scene?”, *International Conference on Computational Photography*, 2013.

[12] A. Azzalini and A. Dalla Valle, “The multivariate skew-normal distribution”, Biometrika Vol. 83, No. 4, pp. 715-726, 1996.

[13] M. C, Jones and A. Pewsey,“Sinh-arcsinh distributions”, *Biometrika* Vol. 96, Iss. 4, pp. 761780, 2009.

[14] M. C, Jones and A. Pewsey, “Sinh-arcsinh distributions: a broad family giving rise to powerful tests of normality and symmetry”, *Technical Report*, The Open University, Department of Statistics. http://statistics.open.ac.uk/TechnicalReports/TechnicalReportsIntro.htm.

[15] F. J. Rubio, E. O. Ogundimu and J. L. Hutton, “Robust modelling using twopiece sinh-arcsinh distributions”, arXiv:1307.6021, 2014.

[16] P. Bortot, ‘’Tail dependence in bivariate skew-Normal and skew-t distributions”, available online: www2. stat. unibo. it/bortot/ricerca/paper-sn-2. pdf, 2010.

[17] C. J. Schuler, M. Hirsch, S. Harmeling, and B/ Schölkopf, “Blind Correction of Optical Aberrations”, *ECCV*, 2012.

[18] S. J. Reeves and R. M. Mersereau, “Blur identification by the method of generalized cross-validation”, *IEEE Trans Image Process.*, Vol. 1, Iss. 3, pp. 301-311, 1992.

[19] G. Pavlovic and A. M. Tekalp, “Maximum likelihood parametric blur identification based on a continuous spatial domain model.”, *IEEE Trans Image Process.* Vol. 1, Iss. 4, pp. 496-504, 1992.

[20] J. P. Oliveira and M. A. T. Figueiredo, “Parametric Blur Estimation for Blind Restoration of Natural Images: Linear Motion and Out-of-Focus”, *IEEE Trans Image Process.* Vol. 23, Iss. 1, pp. 466-77, 2014.

[21] T. S. Cho, A. Levin, A, F. Durand, and W. T. Freeman, “Motion blur removal with orthogonal parabolic exposures”, *IEEE International Conference on Computational Photography*, pp. 1-8, 2010.

[22] R. I. Hartley and A. Zisserman, *Multiple View Geometry in Computer Vision*, Cambridge University Press, 2nd edition, 2004.

[23] E. K. P. Chong and S. H. Zak, *An Introduction to Optimization*, Wiley, 4th edition, 2013.

[24] A. Levin, Y. Weiss, F. Durand, and W. Freeman, “Understanding and evaluating blind deconvolution algorithms”, *IEEE Computer Society Conference on Computer Vision and Pattern Recognition*, pp. 1964-1971, 2009.

[25] M. Afonso, J Bioucas-Dias, M. Figueiredo, “Fast image recovery using variable splitting and constrained optimization, *IEEE Trans. Image Process.*, Vol. 19, Iss. 9, pp. 2345-2356, 2009.

[26] Mahajan, Virendra N., and Viendra N. Mahajan. Aberration theory made simple. Bellingham,, Washington, USA: SPIE optical engineering press, 1991.

[27] Gupta, Arjun K., Graciela Gonzalez-Far?as, and J. Armando Dom?nguez-Molina. ”A multivariate skew normal distribution.” Journal of Multivariate Analysis 89.1 (2004): 181-190.

[28] Sasian, Jose. Introduction to aberrations in optical imaging systems. Cambridge University Press, 2013.